THE JOURNAL OF BIOLOGICAL CHEMISTRY
Vol. 277, No. 34, Issue of August 23, pp. 30976–30983, 2002

Printed in U.S.A.

Crystal Structure of Bacterial Morphinone Reductase and Properties of the C191A Mutant Enzyme*

Received for publication, March 25, 2002, and in revised form, May 28, 2002
Published, JBC Papers in Press, June 3, 2002, DOI 10.1074/jbc.M202846200

Terez Barna‡, Hanan Latif Messiha‡, Carlo Petosa‡§, Neil C. Bruce¶, Nigel S. Scrutton‡‖, and Peter C. E. Moody‡**

From the ‡Department of Biochemistry, University of Leicester, University Road, Leicester LE1 7RH and the ¶Institute of Biotechnology, University of Cambridge, Tennis Court Road, Cambridge CB2 1QT, United Kingdom

The crystal structure of the NADH-dependent bacterial flavoenzyme morphinone reductase (MR) has been determined at 2.2-Å resolution in complex with the oxidizing substrate codeinone. The structure reveals a dimeric enzyme comprising two 8-fold β/α barrel domains, each bound to FMN, and a subunit folding topology and mode of flavin-binding similar to that found in Old Yellow Enzyme (OYE) and pentaerythritol tetranitrate (PETN) reductase. The subunit interface of MR is formed by interactions from an N-terminal β strand and helices 2 and 8 of the barrel domain and is different to that seen in OYE. The active site structures of MR, OYE, and PETN reductase are highly conserved reflecting the ability of these enzymes to catalyze "generic" reactions such as the reduction of 2-cyclohexenone. A region of polypeptide presumed to define the reducing coenzyme specificity is identified by comparison of the MR structure (NADH-dependent) with that of PETN reductase (NADPH-dependent). The active site acid identified in OYE (Tyr-196) and conserved in PETN reductase (Tyr-186) is replaced by Cys-191 in MR. Mutagenesis studies have established that Cys-191 does not act as a crucial acid in the mechanism of reduction of the olefinic bond found in 2-cyclohexenone and codeinone.

The flavoenzyme morphinone reductase (MR)[1] from *Pseudomonas putida* is a member of the Old Yellow Enzyme (OYE) family of proteins (1). MR catalyzes the NADH-dependent saturation of the carbon-carbon bond of both morphinone and codeinone. The products of these reactions, hydromorphone and hydrocodone, are valuable semi-synthetic opiate drugs; hydromorphone is a powerful analgesic (seven times more potent than morphine (2)), and hydrocodone is a mild analgesic and antitussive (3). The synthesis of both compounds is complicated owing to difficulty in specifically oxidizing the C-6 hydroxy group of morphine and the often limiting supply of thebaine (a precursor for the synthesis of hydrocodone). These shortcomings have led to the development of novel recombinant biocatalytic routes for hydromorphone and hydrocodone synthesis (4). Biological synthesis exploits the ability of *Escherichia coli*, transformed with the genes encoding morphinone reductase and morphine dehydrogenase and fed with morphine or codeine, to accumulate hydromorphone and hydrocodone, respectively (5, 6).

MR is a dimeric flavoenzyme of M_r 82,200 (1). It contains one molar equivalent of non-covalently bound FMN per enzyme subunit, and based on sequence similarity studies it belongs to the Class I flavin-dependent β/α barrel oxidoreductases (1, 7). The Class I subfamily includes the isoforms of OYE (8), estrogen binding protein (EBP) from *Candida albicans* (9), pentaerythritol tetranitrate (PETN) reductase (10), glycerol trinitrate reductase (11), the xenobiotic reductases of *Pseudomonas* species (12), and 12-oxophytodienoic acid reductase from tomato (13) and *Arabidopsis thaliana* (14). MR is also related to the more complex bile acid-inducible flavoenzymes Bai H and Bai C (15), the bacterial Fe/S flavoenzymes tri- and dimethylamine dehydrogenases (16, 17), and the NADH oxidase of *Thermoanaerobium brockii* (18). These latter enzymes utilize diverse substrates, but the catalytic framework has clearly evolved from a common progenitor (7).

The crystallographic structures of three members of the Class I subfamily of β/α flavin oxidoreductases have been reported, including that of the complex iron-sulfur flavoprotein trimethylamine dehydrogenase (19, 20). The structures of OYE and a number of ligand complexes of OYE have been reported (21), although the physiological substrate of the enzyme remains elusive. More recently, we reported structures of PETN reductase and complexes of PETN reductase with steroid inhibitors and substrates (22). The folds of both OYE and PETN reductase comprise an 8-fold β/α barrel and reveal the presence of FMN bound at the C-terminal ends of the internal β-strands. The active sites are highly conserved, which reflects the ability of OYE and PETN reductase to reduce the unsaturated bond of a number of 2-cyclic enones (23, 24). Additionally, PETN reductase has been shown to catalyze the denitration of nitroester explosives, the reduction of nitroaromatic explosives such as trinitrotoluene and picrate and degradation of the nitramine explosives (Royal Demolition Explosive (RDX)) (25, 26).

MR shares with the other Class I subfamily members the ability to reduce a number of 2-cyclic enones and to form complexes with steroids (27). However, MR is distinct in its

* This work was supported by grants from the Biotechnology and Biological Sciences Research Council (to P. C. E. M., N. C. B., and N. S. S.), the Wellcome Trust, and the Lister Institute of Preventive Medicine. The costs of publication of this article were defrayed in part by the payment of page charges. This article must therefore be hereby marked "*advertisement*" in accordance with 18 U.S.C. Section 1734 solely to indicate this fact.

The atomic coordinates and structure factors (code 1GWJ) have been deposited in the Protein Data Bank, Research Collaboratory for Structural Bioinformatics, Rutgers University, New Brunswick, NJ (http://www.rcsb.org/).

§ Present address: EMBL Grenoble Outstation, 38042 Grenoble cedex 9, France.

‖ A Lister Institute Research Professor. To whom correspondence may be addressed. Tel.: 44-1-16-223-1337; Fax: 44-1-16-252-3369; E-mail: nss4@le.ac.uk.

** To whom correspondence may be addressed. Tel.: 44-1-16-252-3366; Fax: 44-1-16-252-3473; E-mail: pcem1@le.ac.uk.

[1] The abbreviations used are: MR, morphinone reductase; OYE, Old Yellow Enzyme; PETN, pentaerythritol tetranitrate; EBP, estrogen binding protein; (c-THN)TPN, α-($O^{2'}$-6B-cyclo-1,4,5,6-tetrahydronicotinamide adenine dinucleotide phosphate.

TABLE I

Data collection and refinement statistics for crystals of MR reductase and its complex with codeinone

Values for the outer shells of data are shown in parentheses. For the final model, the parameters are R_{work} (R_{free}), 20.5% (21.6%); number of protein atoms (including FMN), 2917 (390 waters); average *B* factors for protein atoms, 26.9 Å^2; root mean square deviations from ideal bond lengths, 0.01 Å; root mean square deviations from ideal bond angles, 1.3 °.

Dataset	Cu RAXIS IIc	SRS 7.2 MAR180	Cu RAXIS IV
Wavelength (Å)	1.5418	1.488	1.5418
Total reflections	134,821	47,854	73,745
Unique reflections	18,992	20,305	23,548
Cell (Å)	49.6, 121.7, 178.2	47.83, 121.44, 177.78	49.52, 121.34, 178.22
Resolution (Å)	2.5 (2.59)	2.36 (2.44)	2.2 (2.14)
Completeness (%)	99 (97)	91.3 (67.3)	85.1 (69.4)
R_{merge} (%), outer shell	9.2, 24.2	5.7, 24.4	6.3, 29.2
T/σ (T)	26.4 (8.5)	13.7 (3.7)	11.9 (3.1)

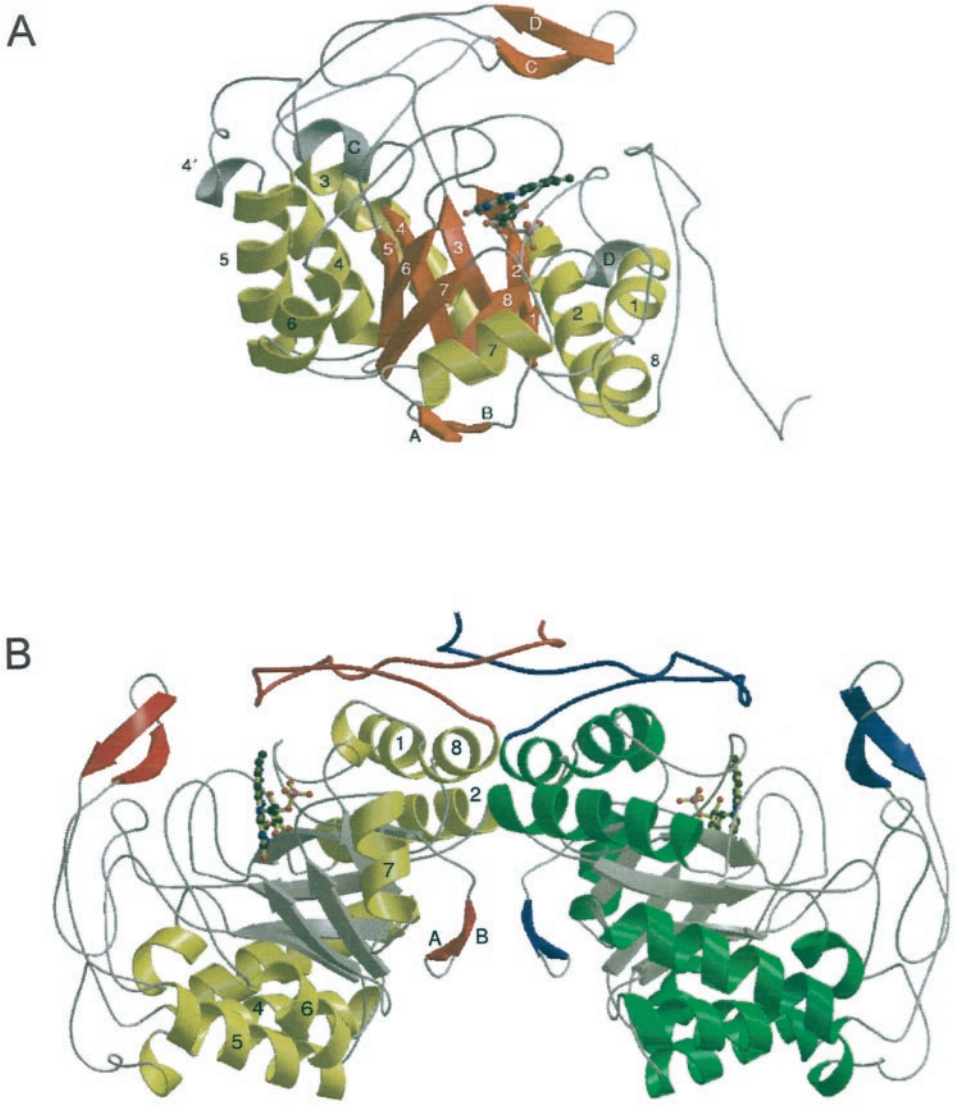

FIG. 1. *A*, structure of a single subunit of MR illustrating the location of the N-terminal cap (β-strands A and B) and the polypeptide excursion incorporating β-strands C and D located between α-helix 3 and β-strand 3 of the barrel core. The location of the FMN cofactor is shown at the C-terminal end of the barrel domain in *ball-and-stick* format. *B*, an orthogonal view of the overall structure of MR illustrating the interactions between the two subunits. Subunit interactions formed by residues in helices 1, 2, and 8 and the external β strands A and B are shown. The graphics image was produced using MOLSCRIPT (46).

ability to reduce the unsaturated carbon-carbon bond of a number of opiate compounds (27). Sequence alignment studies also suggest differences in the chemical nature of the active site of MR compared with OYE and PETN reductase (1). To investigate these aspects, and to provide a structural basis for detailed mechanistic studies of MR, we have solved the structure of MR in complex with the opiate substrate codeinone at 2.2-Å resolution. The structure is discussed in the context of the mechanism of opiate reduction and in view of the existing structural information for PETN reductase and OYE.

EXPERIMENTAL PROCEDURES

Materials—All materials were of analytical grade. Codeinone was a gift from MacFarlan Smith (Edinburgh, Scotland). Mimetic Yellow 2

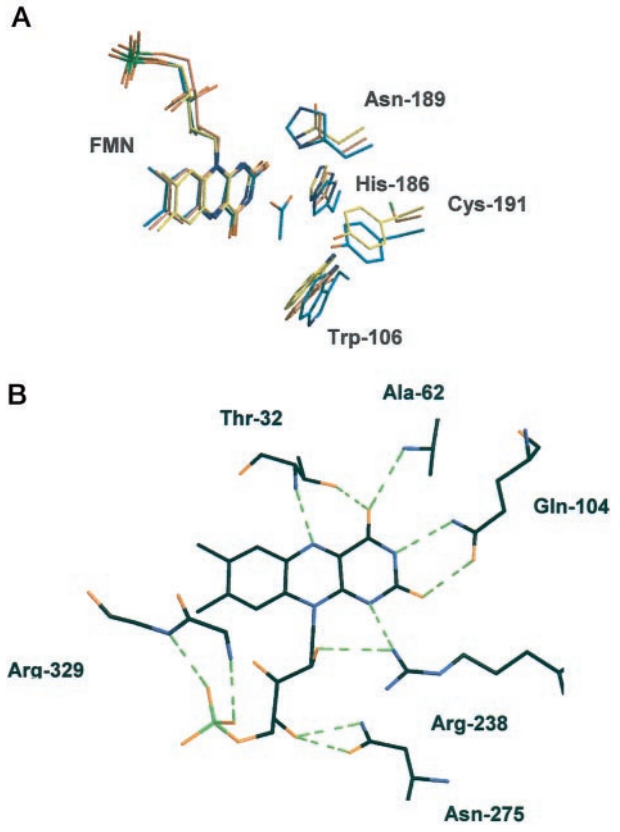

FIG. 2. **Active site structure of MR and protein-flavin interactions in MR.** *A*, superposition of the active sites of MR, OYE, and PETN reductase. The *numbering* of residues is according to that for MR. Asn-189 and His-186 are equivalent to Asn-194 and His-191 of OYE, which are known to be involved in the binding of ligands in the active site of OYE. In PETN reductase the equivalent residue to Asn-189 of MR is a histidine. In OYE and PETN reductase Cys-191 is replaced by tyrosine; this latter group is known to be a proton donor in OYE. Acetate is shown bound to PETN reductase as seen in the crystallographic structure of this enzyme (22). Colors used are: OYE, *yellow*; MR, *magenta*; PETN reductase, *cyan*. *B*, amino acid residues in direct contact with the FMN in MR.

affinity chromatography resin was from Affinity Chromatography Ltd. Q-Sepharose resin was from Amersham Biosciences.

Protein Purification and Mutagenesis—MR was purified from a recombinant strain of *E. coli* expressing the enzyme from the cloned *mor B* gene as described previously (27) but also incorporating a final chromatographic step using Q-Sepharose. In this latter step, enzyme was applied to a Q-Sepharose column (8.5 cm × 5 cm) equilibrated with 30 mM Tris buffer, pH 8.0, containing 2 mM 2-mercaptoethanol (buffer B). The column was washed with 2 liters of buffer B containing 230 mM NaCl and the enzyme was eluted using a gradient of NaCl (250–500 mM) contained in buffer B. For long term storage, MR was kept at −80 °C in 50 mM potassium phosphate buffer, pH 7.0. The C191A mutant MR was isolated using the QuikChange mutagenesis protocol (Stratagene) and the following oligonucleotides: 5′-GTC CAC GCC GCC AAC GCC GCG CTG CCC AAC CAG TTC CTC-3′ and 5′-GAG GAA CTG GTT GGG CAG CGC GGC GTT GGC GGC GTG GAC-3′. Plasmid pMORB3 (1) was used as template for the mutagenesis reactions. The mutant gene was completely sequenced to ensure that spurious changes had not arisen during the mutagenesis reaction. Expression and purification of the C191A MR enzyme was as described for wild-type enzyme.

Crystal Growth—Initial crystallization conditions for the enzyme have been described elsewhere (28), but conditions were refined in the course of the work described here. The optimum crystals were grown from 15–25% monomethyl polyethylene glycol 550, 0.1 M HEPES, 0.1 M NaCl, 1 mM dithiothreitol, pH 6.5–7.5, using the sitting-drop vapor diffusion method. Crystals of the codeinone-enzyme complex were isolated by soaking the crystals in a solution comprising 1 mM codeinone, 10 mM phosphate buffer, and 30% monomethyl polyethylene glycol at pH 6.2 for 20 min. The crystals could be flash-frozen directly, and data were collected in the home laboratory. The crystals belong to space group $I2_12_12_1$ with cell dimensions a = 49.9Å, b = 121.7 Å, and c = 178.2 Å and contain one molecule per asymmetric unit.

X-ray Data Collection—Data sets were obtained from single crystals mounted in rayon loops and cooled to −173 °C in a gas stream of N_2. Three sets of data were used in the course of the work described here. The original data (2.5 Å) were collected using a RAXIS IIc image plate device mounted on a Rigaku rotating anode source with MSC/Yale mirrors. Subsequent 2.36-Å data were recorded at Station 7.2 of SRS (Synchrotron Radiation Source) Daresbury Laboratory with an MAR 180 image plate device, and final 2.2-Å data were recorded using a RAXIS IV image plate device mounted on a Rigaku rotating anode source with MSC/Yale mirrors. Data were processed and reduced using DENZO and SCALEPACK (29). Data statistics are presented in Table I. A random 5% set of the possible reduced data was selected and used to flag reflections for the calculation of free R values (30) in all data sets.

Structure Solution and Refinement—The structure was solved by molecular replacement using AMoRe (31) with a model based on OYE (Protein Data Bank code 1OYA) (21). The correct solutions to the rotation function had the highest peaks with a correlation coefficient of 14.8l; the next highest peaks had a value of 9.5. The translation function solution gave a coefficient of 29.1; this increased to a value of 40.2 upon rigid-body refinement (R = 49.4% for data in the range 20–4.0 Å). The starting model was made using the sequence alignment of French *et al.* (10); all non-conserved side chains were truncated to alanine or glycine ,and all insertions in the OYE sequence were deleted. FMN was not included in these molecular replacement calculations, but calculation of difference maps showed clear density for the cofactor, confirming that the correct solution had been chosen. Subsequent refinement was carried out with XPLOR version 3.843 (32). The model was broken into 12 segments (determined by secondary structure), and each segment was refined as a rigid body. Inspection of sigmaA (33) and $F_o - F_c$ maps was performed with XTALVIEW (34), and rebuilding was followed by simulated annealing and positional refinement. Further rounds of rebuilding and refinement reduced R (R_{free}) for the data for 20–2.5 Å to 36.1% (38.0%) with 80 water molecules. The 2.36-Å data were collected from a crystal soaked with codeinone, and refinement was continued using CNS 0.5 (32). This included further rounds of rebuilding and refinement (both positional and temperature-factor) resulting in a model with R (R_{free}) for data for 40–2.36 Å of 24.5% (28.1%). No interpretable density was seen in the active site, and further codeinone soaking steps were tried. The final 2.2-Å data were collected with a crystal soaked as described above. Refinement with these data used CNS 1.0 (32) and gave final values for R and R_{free} of 20.5% and 21.6%. Codeinone was built into difference density using atomic parameters extracted from the Cambridge Structural Data base through the Chemical Data base Service at Daresbury Laboratory. The parameters for refinement were calculated with XPLOR2D (35). Refinement statistics and final model parameters are presented in Table I. The 2.2-Å data and coordinate files have been deposited with the Protein Data Bank (accession code 1GWJ).

Kinetic Studies—All kinetic studies were performed under strict anaerobic conditions (<5 ppm of O_2) within a glove box environment (Belle Technology) to prevent oxidase activity of MR. Steady-state assays were performed using a Jasco V530 spectrophotometer at 25 °C. Reaction buffer was 50 mM potassium phosphate, pH 7.0, which was made anaerobic by bubbling with humidified Pureshield argon at 5 p.s.i. for 2 h prior to introduction into the glove box. NADH solutions were made from pre-weighed powder and anaerobic buffer inside the glove box, and the concentration was determined spectrophotometrically (ϵ_{340} = 6220 M^{-1} cm^{-1}). Solutions of 2-cyclohexenone were made by dilution of a stock (10 M) into anaerobic buffer. The initial velocity in steady-state assays was determined from absorbance changes at 340 nm in a reaction cell volume of 1 ml; the desired concentration of substrate and cofactor solutions was achieved by making microliter additions to the cell. Least squares fitting procedures to the standard Michaelis-Menten equation were performed using Origin (v6) software (Microcal).

Stopped-flow kinetic experiments were performed under anaerobic conditions using an Applied Photophysics SX.17MV stopped-flow instrument, and transients were analyzed using non-linear least squares regression using Spectrakinetics software (Applied Photophysics). Averages of five to seven individual transients were analyzed. The enzyme was contained in 50 mM potassium phosphate buffer, pH 7.0. In the reductive half-reaction, enzyme (20 μM) was mixed with NADH at different concentrations (at least >5-fold the enzyme concentration to ensure pseudo-first order conditions). Flavin reduction was monitored at 462 nm; formation and decay of the enzyme-NADH charge-transfer

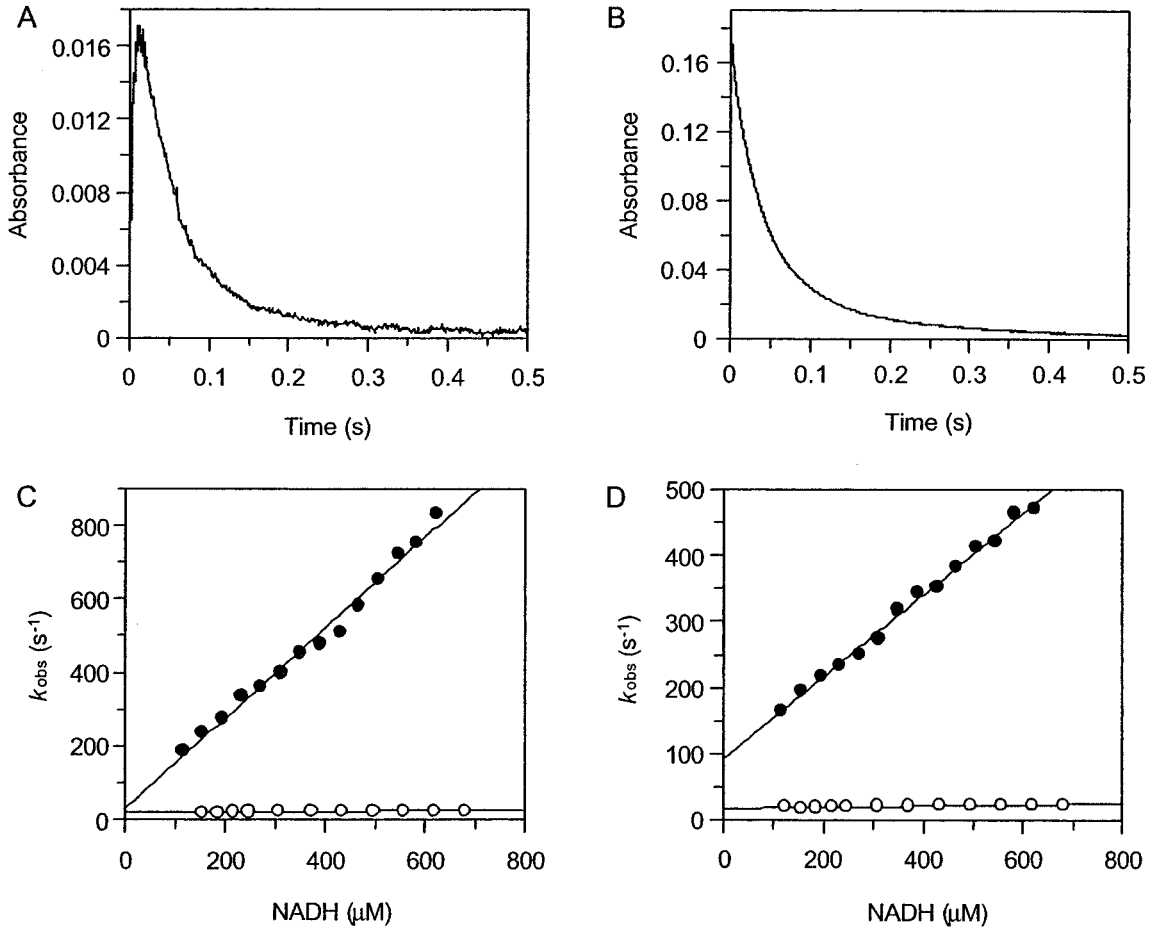

FIG. 3. **Kinetic transients and plots of rate *versus* coenzyme concentration for the reductive half-reactions of wild-type and C191A MR.** Conditions: 50 mM potassium phosphate buffer, pH 7.0; 283 K. *A*, transient observed for the C191A mutant MR at 550 nm; NADH concentration 200 μM. *B*, transient observed at 462 nm for the C191A mutant MR; NADH concentration 200 μM. Similar transients were obtained for wild-type MR, and examples of these can be found in our previous paper (36). *C*, plot of observed rate *versus* NADH concentration for the wild-type enzyme. *Filled circles*, observed rate for formation of the NADH-enzyme charge-transfer species; *unfilled circles*, observed rate for flavin reduction. *D*, same as for *panel C*, but for C191A MR.

TABLE II
Apparent kinetic parameters determined from steady-state assays of wild-type and C191A mutant MR enzymes

Fixed substrate	Wild-type		C191A	
	App. K_m	App. k_{cat}	App. K_m	App. k_{cat}
	mM	s^{-1}	*mM*	s^{-1}
NADH (150 μM)[a]	4.2 ± 0.2	0.80 ± 0.01	8.5 ± 0.4	0.32 ± 0.01
2-cyclohexen-1-one (40 mM)[b]	8.9 ± 0.6	0.88 ± 0.01	12.5 ± 0.9	0.34 ± 0.02

[a] Apparent kinetic parameters are for 2-cyclohexen-1-one.
[b] Apparent kinetic parameters are for NADH.

species was monitored at 552 nm (36). In studies of the oxidative half-reaction, MR was titrated with sodium dithionite to produce the 2-electron-reduced form of MR. Reduced MR (20 μM) was then mixed with 2-cyclohexenone at different concentrations, and flavin oxidation was monitored at 462 nm. Equations used to analyze the reductive half-reaction have been described elsewhere (36). Analysis of the transients obtained for the oxidative half-reaction is described under "Results."

RESULTS AND DISCUSSION

Overall Structure—The structure of MR was determined at 2.2-Å resolution by molecular replacement using OYE as the search model. The structure reveals an 8-fold β/α barrel with non-covalently bound FMN located toward the center and C-terminal end of the barrel (Fig. 1*A*). The overall subunit structure is similar to that reported for OYE (21) and PETN reductase (22). However, it is closer to PETN reductase in that it has a β-loop excursion (comprising of residues 131–151) between β strand 3 and α-helix 3 of the core barrel domain instead of the helix found in OYE. Additionally, β-strands A and B form a cap at the N-terminal domain of the barrel, as seen also in OYE (21) and PETN reductase (22). MR is dimeric, and the structure of the dimer (Fig. 1*B*) reveals that the subunit interactions are different from those reported for OYE (21). In OYE, the dimer interface involves helices 4, 5, and 6 of the β/α barrel, but in MR the interface is less extensive and comprises interactions between the N-terminal β strands (strands A and B, Fig. 1*B*) and helices 2 and 8 of the barrel domain. The dimer interface in MR is not part of the highly conserved region identified by Fox and Karplus in their analysis of OYE (21). In addition, in MR the C-terminal excursion of one subunit extends over the dimer interface and interacts with the corresponding extension from the second subunit (Fig. 1*B*). This C-terminal extension also partially

$$E_{ox} + NADPH \underset{k_{-1}}{\overset{k_1}{\rightleftharpoons}} E_{ox}NADPH \underset{k_{-2}}{\overset{k_2}{\rightleftharpoons}} E_{ox}NADPH^{CT} \underset{k_{-3}}{\overset{k_3}{\rightleftharpoons}} E_{red}NADP^{+} \underset{k_{-4}}{\overset{k_4}{\rightleftharpoons}} E_{red} + NADP^{+}$$

SCHEME 1

$$E_{ox} + NADPH \underset{k_{-1}}{\overset{k_1}{\rightleftharpoons}} E_{ox}NADPH^{CT} \underset{k_{-2}}{\overset{k_2}{\rightleftharpoons}} E_{red}NADP^{+} \underset{k_{-3}}{\overset{k_3}{\rightleftharpoons}} E_{red} + NADP^{+}$$

SCHEME 2

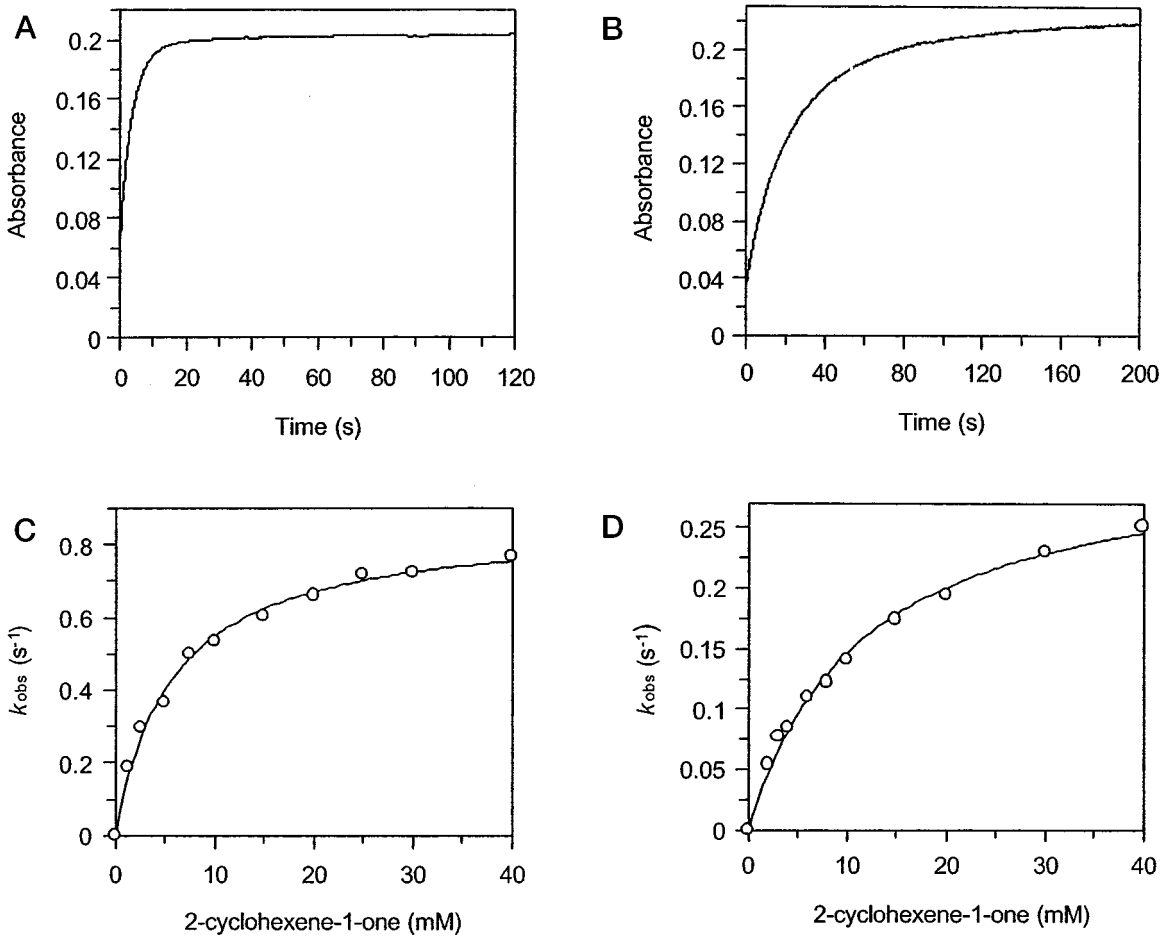

FIG. 4. **Kinetic transients and plots of rate *versus* 2-cyclohexenone concentration for the oxidative half-reactions of wild-type and C191A MR.** Conditions: 50 mM potassium phosphate buffer, pH 7.0; 283 K. *A*, transient observed for wild-type MR at 462 nm; 2-cyclohexenone concentration 2 mM. *B*, transient observed for the C191A mutant MR at 462 nm; 2-cyclohexenone concentration 2 mM. *C*, plot of observed rate (fast phase) *versus* concentration of 2-cyclohexenone. The *solid line* is the fit to the rapid equilibrium formalism of Strickland *et al.* (45); the lack of an intercept on the ordinate axis illustrates the absence of a reverse reaction. *D*, same as for *Panel C* but for C191A mutant MR. See text for kinetic parameters determined from the fitting processes.

defines the entrance to the active site of MR along with the polypeptide excursion found between β strand 3 and α-helix 3 of the core barrel domain.

Active Site Structure in Relation to Other Members of the OYE Family—The active site structure of MR is presented in Fig. 2*A*, alongside those for OYE and PETN reductase. Important differences in the active site of MR can be discerned. Tyr-196 in OYE is known to function as an active site acid in the oxidative half-reaction with α/β unsaturated enones (37). This residue is conserved in PETN reductase (Tyr-186), but in MR the equivalent residue is Cys-191. The active site of MR is larger than the corresponding site in OYE. This is primarily due to the presence of a largely hydrophobic insertion (residues Arg-291 to Glu-301) in OYE that is absent in MR, which lines

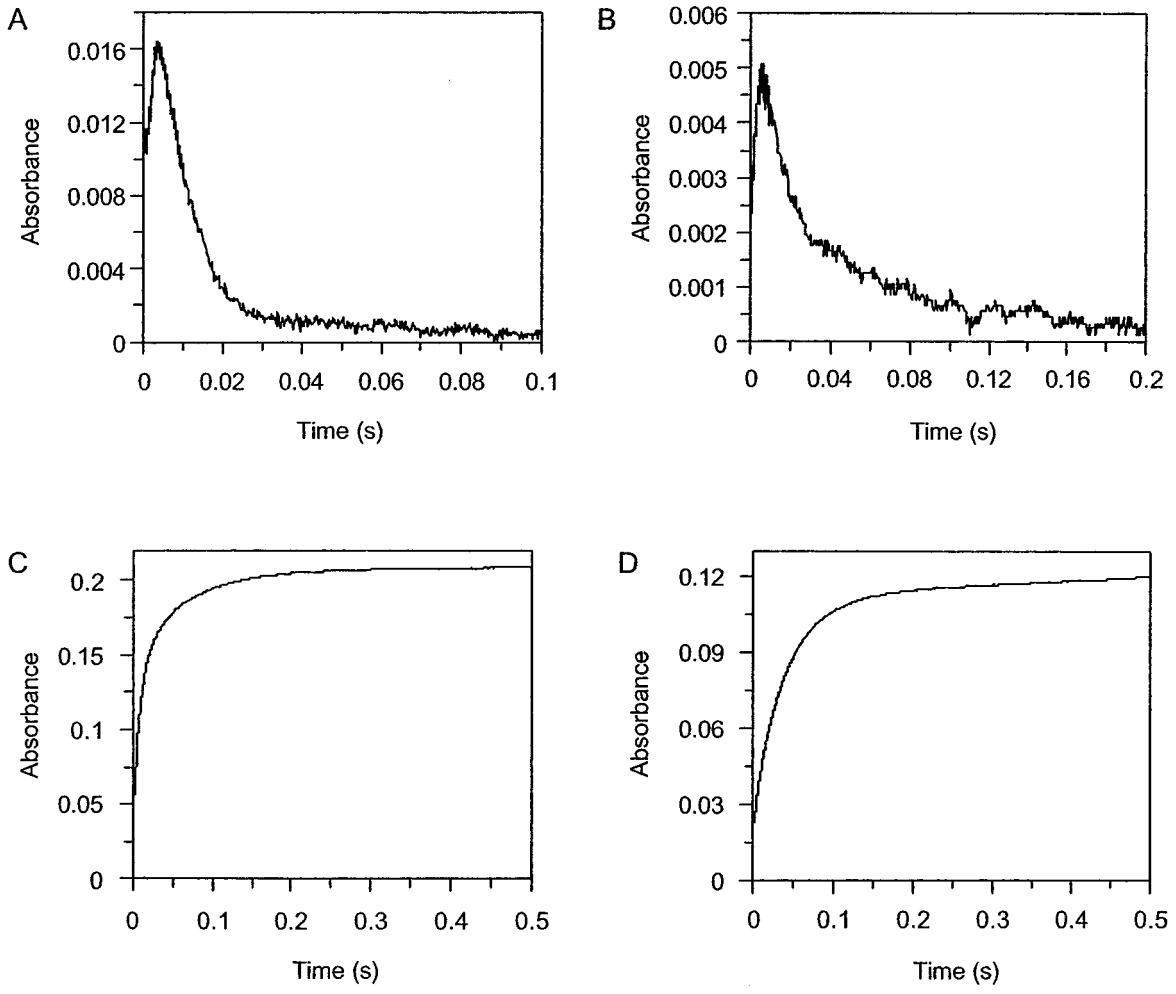

FIG. 5. **Transients obtained for the oxidation of wild-type and C191A MR by codeinone.** Conditions: 50 mM potassium phosphate buffer, pH 7.0; 283 K. *A*, kinetic transient observed at 650 nm for the reaction of NADH-reduced wild-type MR with codeinone (2 mM); fast rate (increase in absorption), 608 s^{-1}, slow rate (decrease in absorption), 119 s^{-1}. *B*, same as for *Panel A* but for C191A MR; fast rate (increase in absorption), 490 s^{-1}, slow rate (decrease in absorption), 40 s^{-1}. *C*, kinetic transient observed at 462 nm for the reaction of reduced wild-type MR with codeinone (2 mM); fast rate (absorption increase), 104 s^{-1}; slow rate (absorption increase), 15 s^{-1}. *D*, same as for *Panel C* but for C191A MR; fast rate (absorption increase), 29 s^{-1}; slow rate (absorption increase), 4 s^{-1}.

the entrance to the active site close to the dimethylbenzene subnucleus of the flavin isoalloxazine ring. Wider access to the active site no doubt reflects the ability of MR to bind more bulky and conformationally restrained substrates such as codeinone and morphinone. His-191 and Asn-194 in OYE, which are involved in ligand binding (21, 38), are conserved in MR as His-186 and Asn-189.

The nature of the flavin contacts in MR (Fig. 2*B*) are essentially identical to those described for OYE, except the O3 atom of the ribityl hydroxyl group is H-bonded to Asn-275 in MR, whereas in OYE this interaction is absent. A key interaction with the flavin is that made by residue Arg-238. The side chain of this group is located close to the N-1/C-2 carbonyl region of the flavin isoalloxazine ring, where it is expected that negative charge will develop during enzyme reduction. Although the positioning of a positively charged side chain in this region in many flavoproteins has been postulated to stabilize developing negative charge (and thus facilitate flavin reduction), our recent mutagenesis studies with MR indicate that Arg-238 is not required to stabilize the reduced flavin (39). This finding is in stark contrast to similar work on lactate monooxygenase, where mutation of the positively charged residue at this region (Lys-266 to Met-266) impairs flavin reduction by substrate (40).

NADH is the natural coenzyme preference of MR. In contrast, PETN reductase, like OYE, has a strong preference for NADPH. The mode of binding NADPH in OYE is not clear; crystallographic studies with the NADP analogue (c-THN)TPN show changes in electron density, but more than one interpretation for the ADP portion has been presented (21). In the absence of a model for coenzyme binding, it is difficult to account for the differences in coenzyme specificity between the family members. Preference for NADPH is often conferred by the presence of two arginine residues in the vicinity of the 2′-phosphate group of the coenzyme (41, 42), although it is important to note that these preferences are derived from a different protein fold. In NADH-dependent dehydrogenases these arginine residues are absent, and an acidic residue (aspartate or glutamate) forms a hydrogen bond to the 2′-hydroxy group of NADH (41, 42). In searching for residues that confer coenzyme preference in the OYE family, we note from modeling studies in which the NMN (nicotinamide mononucleotide) portion of the coenzyme adopts a conformation similar to that seen in OYE (21) that the polypeptide excursion between β-strand 3 and α-helix 3 of the core barrel domain might be positioned appropriately to form interactions with the distal part of the coenzyme. In PETN reductase two arginine residues (Arg-142 and Arg-130) are candidates to confer specificity for NADPH. In contrast, in the NADH-dependent MR these residues are absent and an acidic residue (Glu-135 for MR) is present. We suggest this region of the protein might be important in con-

ferring coenzyme specificity. In OYE, however, the polypeptide excursion between β-strand 3 and α-helix 3 is replaced by a α-helix. If our proposed site for coenzyme recognition is correct, then the mode of interaction of the coenzyme in this region of OYE is different from that in PETN reductase and MR, making general conclusions concerning coenzyme recognition in the family difficult. However, there are a number of acidic and basic residues in this region of OYE that could form interactions with the reducing coenzyme in OYE. Our future studies are now focused on defining those residues that interact with NADH by mutagenesis and kinetic methods.

Crystal Soak Experiments—We have made a number of attempts to soak ligands into the active site of crystalline MR. Our studies have included soaking steps with NADH and the oxidizing substrates 2-cyclohexenone and codeinone. Upon soaking crystals with NADH, the yellow appearance of the crystals fades indicating reduction of the enzyme-bound FMN. This reduction of the flavin occurs without crystal cracking, but analysis of frozen crystals showed no evidence for the presence of coenzyme in the active site. Our observations suggest that $NADP^+$ and NADPH have relatively low affinities for reduced enzyme, consistent with a ping-pong reaction mechanism (27) and with the known moderate affinity of reduced OYE for $NADP^+$ (43). Similarly, analysis of crystals soaked with 2-cyclohexenone showed no evidence of ligand binding in the active site. In contrast, we have had some limited success in analysis of crystals soaked with the oxidizing substrate codeinone. The active site of the MR-codeinone complex clearly shows a large peak of electron density that is not seen in the absence of codeinone. The density is difficult to interpret unambiguously and suggests that codeinone binds in more than one orientation. The density is located over the *si*-face of the flavin in a region similar to that seen with ligands of PETN reductase (22) and OYE (21). Possible interpretations of the density for codeinone are included in the header of the Protein Data Bank entry.

Properties of the C191A Mutant Enzyme—Inspection of the active site of MR and comparison with the active site structures of OYE and PETN reductase reveals that the conventional active site acid (Tyr-196 in OYE and Tyr-186 in PETN reductase) is absent in MR. A common feature of these enzymes is their ability to reduce the olefinic bond of 2-cyclohexenone. The crystal structure of PETN reductase solved in the presence of 2-cyclohexenone reveals that Tyr-186 is ideally placed to protonate the substrate following reduction of the olefinic bond by hydride transfer from the flavin N5 (26) (Fig. 3*A*). Mutagenesis of Tyr-196 in OYE has also confirmed that this residue donates a proton to 2-cyclohexenone in the oxidative half-reaction (37). Given that MR also catalyzes the reduction of the olefinic bond in 2-cyclohexenone, we were interested to learn if Cys-191 (the equivalent of Tyr-196 in OYE and Tyr-186 in PETN reductase) could serve as a proton donor in the reduction of 2-cyclohexenone and codeinone.

Apparent kinetic parameters determined under steady-state conditions using 2-cyclohexenone as oxidizing substrate for both the wild-type and C191A MR enzymes are displayed in Table II. The C191A mutant enzyme retains the ability to reduce 2-cyclohexenone, suggesting that Cys-191 does not play a major role in catalysis. The most pronounced effect on the steady-state kinetic parameters is ~2.5-fold reduction in apparent k_{cat} on converting Cys-191 to alanine. We investigated the kinetics of the reductive and oxidative half-reactions of the wild-type and C191A enzymes to ascertain if the reduction in apparent k_{cat} is associated with impaired flavin reduction or oxidation. Detailed studies of the reductive half-reaction of wild-type MR with NADH as reducing substrate have been reported elsewhere (36) at 278 K, but corresponding studies of the oxidative half-reaction using 2-cyclohexenone as substrate were not reported. Herein, we report the kinetic behavior of both the C191A and wild-type enzyme with NADH, 2-cyclohexenone, and codeinone (determined at 283 K).

The kinetic scheme for the reductive half-reaction is shown in Scheme 1. The minimal kinetic scheme (Scheme 1) is slightly modified compared with that presented in Craig *et al.* (36) (Scheme 2) in that an additional enzyme-NADH complex is shown prior to formation of the enzyme-NADH charge-transfer complex. Inclusion of this complex is consistent with work on OYE (43) and EBP (44), although direct evidence for its formation was lacking in our previous studies with wild-type MR (36). However, our studies with C191A MR suggest that such a species might exist prior to formation of the charge-transfer species (see below). Kinetic transients for flavin reduction and formation of the enzyme-NADH charge-transfer intermediate and plots of observed rate as a function of NADH concentration are shown in Fig. 3 for wild-type and C191A MR. As reported previously for wild-type MR, the rate of formation of the charge-transfer species (observed at 552 nm) is linearly dependent on NADH concentration, whereas the observed rate for flavin reduction is independent of NADH concentration in the range 125–675 μM. The observed rates of flavin reduction for wild-type and C191A MR enzymes are essentially identical (22 and 21 s^{-1}, respectively). The second order rate constant for formation of the charge-transfer species with C191A MR ($6.2 \pm 0.1 \times 10^5$ M^{-1} s^{-1}) is approximately one-half the value measured for wild-type MR ($12.3 \pm 0.4 \times 10^5$ M^{-1} s^{-1}). For Scheme 2, the value of the positive intercept of the ordinate axis (29 ± 14 and 93 ± 8 s^{-1} for wild-type and C191A, respectively) approximates to $k_2 + k_{-1}$. Additionally, the observed rate of flavin reduction (~20 s^{-1} for both enzymes) is independent of NADH concentration (Fig. 3). An approximate value of 9 and 70 s^{-1} for k_{-1} can therefore be estimated for wild-type and C191A, respectively. This gives rise to values of ~7 and ~113 μM, respectively, for the enzyme-NADPH dissociation constant in wild-type and C191A MR. For the wild-type enzyme, the lack of a concentration dependence on the flavin reduction rate in the range 125–675 μM is therefore consistent with Scheme 2 and a dissociation constant for the charge-transfer complex of 7 μM. However, the elevated dissociation constant for the C191A mutant is inconsistent with Scheme 2, because one expects a concentration effect on the flavin reduction rate at relatively low NADH concentrations. The lack of such concentration dependence would be consistent with the more complex Scheme 1, which has been shown for the MR-related enzymes OYE and EBP. Our data for C191A is therefore more consistent with a scheme (Scheme 1) in which a NADH-enzyme complex accumulates prior to formation of the charge-transfer intermediate, where the formation of this complex is rapid (occurring in the dead-time of the stopped-flow apparatus). On the basis of the above arguments it would seem plausible that the same rapid formation of a NADH-enzyme complex prior to formation of the charge-transfer species also occurs in wild-type MR. In this regard, it is important to note that Scheme 1 is not inconsistent with the observed kinetic behavior seen for wild-type MR.

The kinetic behavior of the oxidative half-reaction was investigated using 2-cyclohexenone as oxidizing substrate by mixing with MR that had been reduced at the 2-electron level with dithionite. Recovery of the flavin absorption was observed at 462 nm, and transients were found to be biphasic (Fig. 4). The fast phase contributed >90% of the total amplitude change. Fitting to a standard biphasic expression revealed that the observed rate for this phase was dependent on 2-cyclohexenone concentration, and data were analyzed by fitting to the

rapid equilibrium formalism of Strickland *et al.* (45) (Fig. 4). The observed rate for the slow phase (0.02 and 0.01 s^{-1} for the wild-type and C191A mutant enzymes, respectively) was independent of 2-cyclohexenone concentration, and the origin of this relatively small absorbance change is uncertain. Analysis of the fast phases for the wild-type and C191A MR enzymes using the Strickland equation yielded limiting rate constants of 0.9 ± 0.02 and 0.32 ± 0.01 s^{-1}, respectively. The corresponding dissociation constants for the reduced enzyme-2-cyclohexenone complex are 5.7 ± 0.5 and 11.7 ± 0.9 mM, respectively. The values of the limiting rate constants for flavin oxidation are similar to the apparent k_{cat} values measured under steady-state reactions (Table II). The stopped-flow data indicate, therefore, that flavin oxidation is rate-limiting in steady-state turnover and that mutation of Cys-191 leads to a reduction in k_{cat} by compromising the rate of hydride transfer from the flavin N5 to the olefinic bond of 2-cyclohexenone.

Owing to the very limited supplies of codeinone and difficulties encountered with its stability under stopped-flow conditions, we were unable to conduct an extensive study of the concentration dependence of the oxidative half-reaction with this substrate. However, we were able to collect a small number of kinetic transients for enzyme oxidation by codeinone. Fig. 5 illustrates kinetic transients obtained by mixing 2-electron-reduced MR (*i.e.* enzyme reduced with a stoichiometric concentration of NADH) with codeinone (2 mM). At 650 nm, a charge-transfer species accumulates prior to hydride transfer to codeinone (consistent with our previous work with wild-type MR (36)) for both wild-type and C191A MR. The formation of the charge-transfer species occurs with similar kinetics in both enzymes (608 and 490 s^{-1} for wild-type and C191A, respectively). Flavin re-oxidation observed at 462 nm gives rise to biphasic transients; the rates of both phases are ~4-fold less in C191A MR, but it is important to emphasize that these are not limiting rate constants. The transients indicate, however, that mutation of Cys-191 does not substantially impair the oxidative half-reaction when codeinone is used as the oxidizing substrate. Reactions with codeinone are faster than with 2-cyclohexenone by a factor of about 10^3, suggesting that the olefinic bond of codeinone is more optimally aligned with the flavin N5 atom in reduced enzyme compared with the olefinic bond in 2-cyclohexenone. Our data rule out the possibility that Cys-191 acts as a crucial active site acid in the mechanism of reduction of 2-cyclohexenone and codeinone. The identity of the key acid will be explored in future studies by mutagenesis and kinetic studies.

Concluding Remarks—At the subunit level, the structure of MR reveals a close structural similarity with OYE and PETN reductase, but the interactions that direct subunit-subunit association are fundamentally different from those reported for OYE. Comparison of the structures of PETN reductase (NADPH-specific) and MR (NADH-specific) suggest a region located in a polypeptide excursion between β-strand 3 and α-helix 3 of the core barrel domain that might confer specificity for the reducing coenzyme. Superposition of the structure of MR with that of OYE and PETN reductase reveals a high degree of conservation within the active site, reflecting the ability of this family of enzymes to reduce "generic" substrates such as 2-cyclohexenone. The active site acid (Tyr-196 and Tyr-186 in OYE and PETN reductase, respectively) is not conserved in MR and is replaced by Cys-191. Mutagenesis studies reveal that Cys-191 does not play a crucial role in the reductive or oxidative half-reactions of MR, thus ruling out a key role as an acid in the reduction of olefinic substrates. A number of alternative potential residues in the active site of MR may serve as the crucial active site acid required for reduction of the olefinic bond in 2-cyclohexenone and codeinone.

REFERENCES

1. French, C. E., and Bruce, N. C. (1995) *Biochem. J.* **312,** 671–678
2. Melmon, K., and Morrelli, H. (1972) *Clinical Pharmacology: Basic Principles in Therapeutics*, Macmillan Publishing Co., New York
3. Moffat, A., Jackson, J., Moss, M., and Widdop, B. (1986) *Clarke's Isolation and Identification of Drugs*, The Pharmaceutical Press, London
4. Bruce, N., French, C., Hailes, A., Long, M., and Rathbone, D. (1995) *Trends Biotechnol.* **13,** 200–205
5. French, C. E., Hailes, A. M., Rathbone, D. A., Long, M. T., Willey, D. L., and Bruce, N. C. (1995) *Bio/Technology* **13,** 674–676
6. Willey, D. L., Caswell, D. A., Lowe, C. R., and Bruce, N. C. (1993) *Biochem. J.* **290,** 539–544
7. Scrutton, N. S. (1994) *Bioessays* **16,** 115–122
8. Stott, K., Saito, K., Thiele, D. J., and Massey, V. (1993) *J. Biol. Chem.* **268,** 6097–6106
9. Madani, N. D., Malloy, P. J., Rodriguez-Pombo, P., Krishnan, A. V., and Feldman, D. (1994) *Proc. Natl. Acad. Sci. U. S. A.* **91,** 922–926
10. French, C. E., Nicklin, S., and Bruce, N. C. (1996) *J. Bacteriol.* **178,** 6623–6627
11. Snape, J. R., Walkley, N. A., Morby, A. P., Nicklin, S., and White, G. F. (1997) *J. Bacteriol.* **179,** 7796–7802
12. Blehert, D. S., Fox, B. G., and Chambliss, G. H. (1999) *J. Bacteriol.* **181,** 6254–6263
13. Strassner, J., Furholz, A., Maceroux, P., Amrhein, N., Schaller, A., Schaller, F., and Weiler, E. (1999) in *Flavins and Flavoproteins* (Ghisla, S., Kroneck, P., Macheroux, P., and Sund, H., eds) pp. 655–658, Rudolf Weber, Berlin
14. Schaller, F., and Weiler, E. W. (1997) *J. Biol. Chem.* **272,** 28066–28072
15. Franklund, C. V., Baron, S. F., and Hylemon, P. B. (1993) *J. Bacteriol.* **175,** 3002–3012
16. Boyd, G., Mathews, F. S., Packman, L. C., and Scrutton, N. S. (1992) *FEBS Lett.* **308,** 271–276
17. Yang, C. C., Packman, L. C., and Scrutton, N. S. (1995) *Eur. J. Biochem.* **232,** 264–271
18. Liu, X. L., and Scopes, R. K. (1993) *Biochim. Biophys. Acta* **1174,** 187–190
19. Lim, L. W., Shamala, N., Mathews, F. S., Steenkamp, D. J., Hamlin, R., and Xuong, N. H. (1986) *J. Biol. Chem.* **261,** 15140–15146
20. Trickey, P., Basran, J., Lian, L. Y., Chen, Z., Barton, J. D., Sutcliffe, M. J., Scrutton, N. S., and Mathews, F. S. (2000) *Biochemistry* **39,** 7678–7688
21. Fox, K. M., and Karplus, P. A. (1994) *Structure* **2,** 1089–1105
22. Barna, T., Khan, H., Bruce, N., Barsukov, I., Scrutton, N., and Moody, P. (2001) *J. Mol. Biol.* **310,** 433–447
23. Vaz, A. D., Chakraborty, S., and Massey, V. (1995) *Biochemistry* **34,** 4246–4256
24. Williams, R. E., Rathbone, D., Bruce, N. C., Scrutton, N. S., Moody, P. C. E., and Nicklin, S. (1999) in *Flavins and Flavoproteins* (Ghisla, S., Kroneck, P., Macheroux, P., and Sund, H., eds) pp. 663–666, Rudolf Weber, Berlin
25. Williams, R., Rathbone, D., Moody, P., Scrutton, N., and Bruce, N. (2001) *Biochem. Soc. Symp.* **68,** 143–153
26. Khan, H., Harris, R. J., Barna, T., Craig, D. H., Bruce, N. C., Munro, A. W., Moody, P. C. E., and Scrutton, N. S. (2002) *J. Biol. Chem.* **277,** 21906–29012
27. French, C. E., and Bruce, N. C. (1994) *Biochem. J.* **301,** 97–103
28. Moody, P. C. E., Shikotra, N., French, C. E., Bruce, N. C., and Scrutton, N. S. (1997) *Acta Crystallogr. Sect. D Biol. Crystallogr.* **53,** 619–621
29. Otwinowski, Z., and Minor W. (1997) *Methods Enzymol.* **276,** 307–326
30. Brunger, A. (1997) *Methods Enzymol.* **277,** 366–396
31. Navaza, J. (1994) *Acta Crystallogr. Sect. A* **50,** 157–163
32. Brunger, A., Adams, P., Clore, G., DeLano, W., Gros, P., Grosse-Kunstleve, R., Jiang, J.-S., Kuszewski, J., Nilges, M., Pannu, N., Read, R., Rice, L., Simonson, T., and Warren, G. (1998) *Acta Crystallogr. Sect. D Biol. Crystallogr.* **54,** 905–929
33. Read, R. (1986) *Acta Crystallogr. Sect. A* **42,** 140–149
34. McRee, D. (1992) *J. Mol. Graphics* **10,** 44–46
35. Kleywegt, G., and Jones, T. (1998) *Acta Crystallogr. Sect. D Biol. Crystallogr.* **54,** 1119–1131
36. Craig, D. H., Moody, P. C. E., Bruce, N. C., and Scrutton, N. S. (1998) *Biochemistry* **37,** 7598–7607
37. Kohli, R. M., and Massey, V. (1998) *J. Biol. Chem.* **273,** 32763–32770
38. Brown, B. J., Deng, Z., Karplus, P. A., and Massey, V. (1998) *J. Biol. Chem.* **273,** 32753–32762
39. Craig, D. H., Barna, T., Moody, P. C., Bruce, N. C., Chapman, S. K., Munro, A. W., and Scrutton, N. S. (2001) *Biochem. J.* **359,** 315–323
40. Muh, U., Massey, V., and Williams, C. H., Jr. (1994) *J. Biol. Chem.* **269,** 7982–7988
41. Scrutton, D. R., Robson, P., and Davies, R. M. (1967) *Nature* **213,** 950–952
42. Bocanegra, J. A., Scrutton, N. S., and Perham, R. N. (1993) *Biochemistry* **32,** 2737–2740
43. Massey, V., and Schopfer, L. M. (1986) *J. Biol. Chem.* **261,** 1215–1222
44. Buckman, J., and Miller, S. M. (1998) *Biochemistry* **37,** 14326–14336
45. Strickland, S., Palmer, G., and Massey, V. (1975) *J. Biol. Chem.* **250,** 4048–4052
46. Kraulis, P. J. (1991) *J. Appl. Crystallogr.* **23,** 946–949